Climatic Change (2021) 166: 41
https://doi.org/10.1007/s10584-021-03131-y

Meteorological drought and its large-scale climate patterns in each season in Central Asia from 1901 to 2015

Xuezhen Zhang [1,2] · Miao He [1,2] · Mengxin Bai [1,2] · Quansheng Ge [1]

Received: 27 October 2020 / Accepted: 17 May 2021 / Published online: 15 June 2021

Abstract
The long-term variations in meteorological drought and its large-scale climate patterns in each season in Central Asia from 1901 to 2015 remain unclear. Here, this issue is addressed using meteorology measurements and reanalysis data through correlation and composite analyses. The drought intensity index (DII) and extent index (DEI) do not exhibit significant linear trends from 1901 to 2015 but do exhibit interannual to interdecadal variations. Both the DII and DEI are highly correlated with the tropical Niño 4 sea surface temperature (SST) and extratropical atmospheric teleconnections, including the East Atlantic (EA) pattern, the East Atlantic/West Russia (EAWR) pattern, and the Arctic oscillation (AO), but with seasonal discrepancies in terms of the degree of influence. The winter drought is strongly linked to both the negative EA and negative EAWR patterns, while spring and autumn drought are strongly linked to the negative EAWR and negative EA patterns, respectively. In the winter, spring, and autumn, drought is also closely linked to below normal Niño 4 SST. The links to EA and EAWR patterns are mainly derived from their impacts on precipitation in the central and northern sectors, while the link to Niño 4 SST is mainly derived from its impacts on precipitation in the southern sector. By considering both drought intensity and drought extent, the ten extreme drought years for each season are selected and, through composite analysis, their large-scale climate patterns are studied. The extreme drought generally occurs in the contexts of a negative EA pattern in winter, a negative EAWR pattern in spring, and a negative AO pattern in autumn. As an exception, summer drought is weakly correlated with Niño 4 SST and is not correlated with extratropical atmospheric teleconnections.

Keywords Meteorological drought · Large-scale climate pattern · Central Asia · Twentieth century

✉ Quansheng Ge
geqs@igsnrr.ac.cn

Extended author information available on the last page of the article

1 Introduction

A drought is predominantly characterized by a prolonged water deficit, and is more than a physical phenomenon or natural event, as it may have serious impacts on agriculture, water resources, ecosystems, and society (Vicente-Serrano et al. 2020). Few natural hazards are as economically, ecologically, and socially disruptive as droughts, which can lead to food and water shortages that threaten national security (Sugg et al. 2020). There are generally four categories of droughts: meteorological, agricultural, hydrological, and socioeconomic droughts (Heim 2002). Among them, meteorological droughts are characterized by below normal precipitation and usually trigger other types of droughts. Meteorological droughts are also mostly linked to large-scale atmospheric circulation anomalies, which are closely related to global climate change. It is thereby an important bridge linking climate change and its impacts on humans.

Central Asia is located far from the ocean and has an arid and semiarid climate with little precipitation but high evaporation (Barlow et al. 2016). It frequently suffers from drought disasters under global climate warming (Lioubimtseva and Henebry 2009). The impacts of large-scale climate patterns anomaly on droughts in Central Asia have been studied by many researchers. These studies show that droughts in Central Asia are modulated by many large-scale atmospheric circulation patterns and sea surface temperatures (SSTs). For instance, Hu et al. (2017) reported that the regional mean annual precipitation of Central Asia was positively correlated with the ENSO index but not significantly correlated with the North Atlantic oscillation (NAO) or Arctic oscillation (AO). Guo et al. (2018a) reported that the annual standard precipitation and evapotranspiration index (SPEI), which represents the combined effects of precipitation and temperature, is strongly associated with ENSO and is also significantly modulated by the NAO for most subregions of Central Asia. Xu et al. (2019) reported that from March–September in Xinjiang, China, in the eastern region of Central Asia, droughts mostly occurred in the context of negative NAO pattern, which may weaken the westerlies and hence reduce the water vapor supply to Central Asia.

At the seasonal scale, the large-scale climate patterns potentially leading to droughts in Central Asia are complicated (Bothe et al. 2012; Guan et al. 2019). Bothe et al. (2012) highlighted the importance of Eurasian wave trains represented by the East Atlantic/Western Russia (EAWR) and Scandinavian (SCAND) patterns with seasonal variations in the regional precipitation of the southeastern region of Central Asia. de Beurs et al. (2018) reported that spring precipitation over more than half of Central Asia is positively correlated with the last winter ENSO index and spring SCAND index, while very few areas of summer precipitation are correlated with these large-scale climate patterns. Over the southern-central area of Central Asia, summer precipitation is closely correlated with summer SST in the tropical Indian Ocean, where anomalously warm SSTs favor southerlies carrying warm and moist air masses to Central Asia (Zhao et al. 2014; Zhou et al. 2015; Zhao and Zhang 2016). Tao et al. (2014) also found that warm season wet anomalies in the Tarim River Basin in the southeastern region of Central Asia generally occurred in the context of intensified water vapor from the Arabian Sea and the Bay of Bengal. However, Hua et al. (2017) reported that precipitation in the northwestern corner of China, which is the northeastern region of Central Asia, was mainly derived from the North Atlantic, and the wet anomaly occurred in the context of positive NAO pattern as well as anticyclonic circulation over Europe and a cyclonic anomaly over Central Asia. Guan et al. (2019) confirmed that water vapor in Central Asia was mainly derived from the Atlantic Ocean and high latitudes of the European continent in summer.

These studies shows precipitation in Central Asia is modulated by both extratropical atmospheric oscillations and tropical ocean-atmosphere interactions. However, the seasonal discrepancies in the dominant large-scale climate patterns that modulate precipitation, in particular that lead to extremely low precipitation, in Central Asia have been rarely studied and, thus, it remains unclear. Some existing studies relevant to seasonal precipitation mostly paid attention to the eastern and southern sectors of Central Asia, including Xinjiang, China, but the western and northern regions were less studied. The precipitation climatology in western Central Asia is largely different from that in eastern Central Asia (Schiemann et al. 2008; Guan et al. 2019). In summary, long-term variations of drought for the entire Central Asia region over the twentieth century and their link to large-scale climate patterns, in particular discrepancies among the seasons, have not yet been understood very clearly. Our ability to predict future drought are hence limited to a certain extent.

The main body of Central Asia is occupied by the five Central Asian states of the former Soviet Union, i.e., Turkmenistan, Uzbekistan, Tajikistan, Kyrgyzstan, and Kazakhstan. These areas are vulnerable to drought due to relative underdevelopment resulting from an economic focus on monoculture agricultural exports before 1991 and traumatic social, economic, and institutional upheavals following independence (Lioubimtseva and Henebry 2009). Conflicts induced by water shortages have become the main factors threatening the national security and stability of Central Asian countries (Farah 2015). Knowledge of the large-scale climate patterns linked with drought is particularly important for these areas.

Therefore, the five Central Asian states of the former Soviet Union were chosen as the study area of this research (Fig. S1). The aim is to depict the large-scale climate patterns linked with regional droughts, particularly extreme droughts, and their seasonal discrepancies. This study consists of two tasks: (1) quantifying regional drought variations and (2) exploring the large-scale atmospheric circulations, ocean-atmosphere interactions and SST anomalies linked with the regional droughts for each season. The remainder of this paper is organized as follows. The second section introduces the dataset sources and methodology. Then, the results are presented in the third section. The fourth section discusses the implications of our results by comparing to existing studies as well as discusses potential future research directions. Finally, the whole study is summarized in the fifth section.

2 Data and methods

2.1 Study area and data sources

The study area is dominated by the westerly climatic regime (Bothe et al. 2012; Chen and Huang 2017). Located in an area with low moisture at mid to low latitudes, water vapor transport is characterized by input along the western and southern boundaries and output along the eastern boundary (Guan et al. 2019; Fig. S1). The precipitable water vapor content (PWC) over the study area is mainly characterized by a seasonal cycle with a minimum in winter (January) and a maximum in summer (July), while the seasonal cycles of precipitation are characterized by a peak in spring (March to May) and low values from summer to autumn, particularly with a minimum in September (Schiemann et al. 2008; Guan et al. 2019). For the southern four states, i.e., Uzbekistan, Turkmenistan, Tajikistan, and Kyrgyzstan, spring precipitation accounts for as much as approximately 40% of annual total precipitation, while summer (June to August) precipitation accounts for only approximately 10% (Guan et al.

2019). Hence, there are remarkable mismatches in the seasonal cycles between the PWC and precipitation.

This study used ground measurements of meteorological data, i.e., the CRU TS dataset v4.03, provided by the Climate Research Unit (CRU) from the University of East Anglia (available at http://http://www.cru.uea.ac.uk/data). This dataset covers the period from 1901 to 2015 with a monthly interval and a grid size of 0.5° by 0.5°. As a gauge-interpolated dataset, the CRU precipitation dataset is generated from different gauge datasets, including the Monthly Climatic Data for the World (MCDW), monthly climate bulletins, World Weather Records data, and some other monthly climate datasets with good quality control and homogeneity checks (Mitchell and Jones 2005; Harris et al. 2014). CRU datasets have been widely applied in climatological studies in Central Asia (e.g., Deng and Chen 2017; Li et al. 2016). By comparing to ground gauge-based measurements, Hu et al. (2018) reported that among the three most widely used precipitation datasets, i.e., Global Precipitation Climatology Centre (GPCC) V7, CRU TS 3.22, and Willmott and Matsuura (WM) precipitation data, the CRU dataset has the best performance in capturing drought events in Central Asia.

This study also used geopotential height data from the NOAA-CIRES twentieth Century Reanalysis dataset (Slivinski et al. 2019), which covers the period from 1871 to 2012. This reanalysis assimilated only surface observations of synoptic pressure, monthly SST, and sea ice distribution. The model used for the assimilation was the 2008 experimental reduced-resolution version of the NCEP Global Forecast System (GFS2008ex), which has a horizontal resolution of nearly 200 km and 28 levels in the vertical direction (for more detail, see http://www.esrl.noaa.gov/psd/data/gridded/data.20thC_ReanV2c.html).

A group of indices for large-scale atmospheric circulations, ocean-atmosphere interactions, and sea surface temperature (SST) anomalies were also used. In terms of atmospheric circulation, the Arctic oscillation (AO), North Atlantic oscillation (NAO), East Atlantic (EA) pattern, East Atlantic/West Russia (EAWR) pattern, Polar/Eurasia (POEA) pattern, and Scandinavia (SCAND) pattern were considered. On behalf of ocean–atmosphere interactions, the Pacific decadal oscillation (PDO) and the Atlantic multidecadal oscillation (AMO) were considered; on behalf of SST anomalies, the Niño 3.4 SST and the Niño 4 SST were considered. All indices were derived from https://www.esrl.noaa.gov/psd/data/climateindices/list/ (see Table S1 for more details).

2.2 Method

In the first part, precipitation was converted into standard precipitation indices (SPIs) for winter (December to February), spring (March to May), summer (June to August), and autumn (September to November). For each season, the SPI was calculated at a time scale of three months. The SPI is one of the most popular drought indices (Damberg and AghaKouchak 2014) because it is applicable to different time scales, simple to calculate, and allows for easy comparison between different climate regimes (Ashraf and Routray 2015; Ganguli and Ganguly 2016). The SPI approximately follows the normal distribution. The conversion from precipitation to SPI removes the effects of skewed precipitation distributions.

Next, as the measurement metrics of regional droughts, two indices were constructed based on the SPI. One index is the regional drought intensity index (DII), and the other index is the regional drought extent index (DEI). Drought is a land phenomenon characterized by a water deficit status within a certain domain and period. There may be large discrepancies among drought events in terms of the extent of the water deficit, duration, and spatial domain (e.g.,

Sheffield et al. 2009). Therefore, to comprehensively quantify drought events, three dimensions consisting of the spatial dimension, temporal dimension, and intensity dimension are needed. Following this idea, the severity–area–duration (SAD) method was proposed (Andreadis et al. 2005). The three-dimensional joint method performs more comprehensively than the traditional method with only one dimension, i.e., regional mean intensity with the spatial dimension excluded (see review by Zhai et al. 2017). This study was performed to quantify the regional drought status for each season rather than for individual drought events. Therefore, the duration of one individual event was discarded, and both the spatial extent indicated by the DEI and the severity indicated by the DII were applied jointly.

The DII was defined as the lower 10% quantile of the accumulated SPI frequencies of all grid cells within the study area for each year. In detail, the SPI of all grid cells was fitted with the normal distribution model, and the lower 10% quantile was estimated. Since the values in the lower 10% quantile are usually negative, a lower DII represents a more severe drought. According to the definition of the DII, it differs from the regional mean SPI. The regional mean SPI aggregates the information of all grid cells within this region. Precipitation is well known to be characterized by large spatial variability. It is usual that precipitation is below normal in one area while above normal in a nearby area. As a consequence, the regional mean would be normal due to offseting each other. However, the DII may avoid this shortcoming. The DII could not only represent the intensity of drought over large areas but also indicate the intensity of drought over small areas.

The DEI was defined as the fraction of drought-bearing grid cells to the total number of grid cells within the study area (Eq. (1)). The drought-bearing grid cells were defined as where SPI was below the lower 10% quantile of the accumulated SPI frequencies throughout the study period. In detail, the yearly SPI values throughout the study period were fitted with the normal distribution model, and the years that fell below the lower 10% quantile were marked as drought-bearing. For each year, the number of grid cells with drought markers were calculated and the fraction to the total number of grid cells within the study area was calculated. An intensified DEI (hereafter, it is named DEI Plus) was also calculated with the same method but with the threshold value of lower 5% quantile to select drought-bearing grid cells. For most of the existing studies based on SPI, the drought extent was quantified by the areas with SPI values lower than a threshold value that was exactly the same among all grid cells (e.g., Zhai et al. 2017). This study used the lower 10% quantile (SPI_{0j} in Eq. (2)), which differed from one grid cell to another due to the geographic differences in precipitation. By applying the lower 10% quantile as the threshold value, the geographic differences in drought criteria were thereby considered.

$$DEI_i = \sum_{j=1}^{N} X_{ij}/N \tag{1}$$

where

$$X_{ij} = \begin{cases} 0, SPI_{ij} > SPI_{0j} \\ 1, SPI_{ij} \leq SPI_{0j} \end{cases}, \tag{2}$$

where i denotes the year, j denotes pixels within the study area, and SPI_{0j} denotes the lower 10% quantile of SPI at grid cell j throughout the study period ($i = 1, \ldots, 104$), which was estimated by fitting SPI_{ij} with the normal distribution model.

In the second part, the Pearson correlation was used to measure the relationships between drought and large-scale climate patterns, including atmospheric circulation, ocean-atmosphere

interactions as well as SST anomalies. The Pearson correlation is a useful and common method to measure the potential effect of one variable on another variable. Additionally, the composite analysis method was used to depict large-scale climate pattern anomalies when severe regional drought events occur. Composite analysis is also often a useful technique to determine some of the basic structural characteristics of a meteorological or climatological phenomenon that occurs over time. Composite analysis involves collecting large numbers of cases of a given meteorological phenomenon. Herein, the ten extreme drought years from 1901 to 2015 for each season were selected by considering both the DII and DEI; then, the large-scale climate pattern anomalies for the ten drought years referring to the climatology mean climate patterns of the other years ($n = 104$) were depicted.

3 Results

3.1 Regional drought intensity and extent variations

Figure 1 shows the DII and DEI variations for each season. For winter, the variations in regional drought intensity in the study period were characterized by decadal fluctuations. From the 1900s to 1960s, the DII decreased with a slope of -0.075 ± 0.073/10a (95% confidence interval; hereafter the same). Regional drought intensity developed gradually. It reached a peak, which was indicated by lowest DII at decadal scale, in the 1960s. Thereafter, from the 1970s to 1990s, the DII exhibited an upward trend; then, it was replaced by another declining trend beginning in 2000. As a result, the decadal DII reached a peak in the 1990s, which was comparable to that in the 1900s.

The variations in regional drought extent also exhibited decadal fluctuations. From 1902 to 1970, the DEI developed gradually with a slope of 0.01 ± 0.015/10a. The decadal DEI reached its peak in the 1950s. Thereafter, the DEI declined and reached a minimum in the 1990s. Since 2000, the DEI again exhibited an upward trend but with a lesser slope than that before 1970.

For spring, the regional drought intensity essentially weakened, with a DII slope of 0.04 ± 0.037/10a (Fig. 1b). Meanwhile, there were also decadal fluctuations with low values, i.e.,

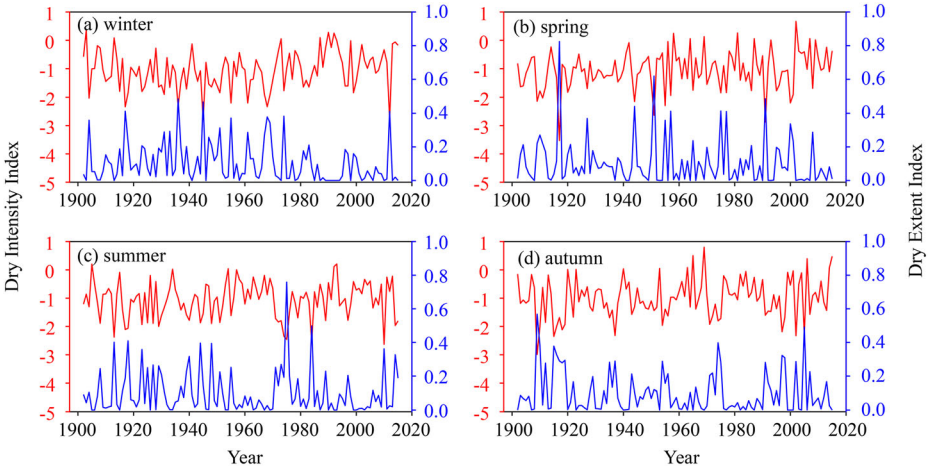

Fig. 1 Annual variations in the drought extent index (DEI) and drought intensity index (DII) from 1902 to 2015

intensified drought, in the 1990s and high values, i.e., weakened drought, in the 1960s. However, from 1902 to 2015, there was no significant trend for the DEI. At the decadal scale, the drought extent was large in the 1950s and 1990s and small in the 1960s.

For summer, both the DEIs and DIIs had non-significant trends but with evident decadal fluctuations (Fig. 1c). There was a low DII, indicating intensified drought, during the 1910s, 1920s, 1940s, 1970s, 1980s, and 2010s. The DII reached the minimum in the 1970s, indicating the most intense drought. Along with the low DII values, there were high DEI values, indicating extensive drought in these decades. The DEI grew to its peak, indicating the most extensive drought in the 1970s. It suggests that the most severe and extensive droughts mainly occurred in the 1970s. In particular, in 1975, the DII decreased to as low as −2.5, and the DEI increased to as high as 0.75.

For autumn, there were also decadal fluctuations in both the DII and DEI (Fig. 1d). The DII exhibited an increasing trend before the 1960s and a declining trend after the 1960s; however, an increasing trend occurred again after the 1990s. The phases of the DEI variations were approximately opposite to the DII variations. The DEI showed a declining trend before the 1960s and an increasing trend after the 1960s, which was replaced by a declining trend after 2000. These findings indicate that the droughts in the 1900s and 1990s were more intense and extensive than those in the other decades.

The abovementioned results demonstrate that both the drought intensity and drought extent variations from 1902 to 2015 were mainly characterized by both interannual variations and decadal variations but with seasonal discrepancies. In particular, at the decadal scale, the DII in spring and autumn shared an approximately similar trends shift of "uptrend–decline–uptrend," but in winter there was a trend shift of "decline–uptrend–decline." The trend shift of the DEI was approximately opposite to that of the DII. As a result, severe and extensive droughts mostly occurred in the mid-twentieth century for winter and summer, while they occurred in the early twentieth century and late twentieth century for spring and autumn.

3.2 Extreme drought years

Following the definitions of the DII and DEI, the points in the bottom-right corner of the plot and with dark red color in Fig. 2 denote the extreme drought years. For winter, 1945 was prominently characterized by both a large DEI and a low DII. The DEI in 1945 was 0.46, which was larger than the value of 0.41 in 2012; the DII in 1945 was −2.79, which was lower than the value of −2.3 in 1936. The years 1936 and 2012 were characterized by large DEI values and low DII values, respectively. Following these years, 1917, 1968, and 1955 were the most extreme drought years; finally, we selected the ten extreme drought years (Table S2). For spring, the most extreme drought year was 1917, followed (in decreasing order of severity) by 1951, 1991, and 1944 (Table S2). For the summer, there were comparable DIIs in 1975, 1984, 2010, and 1913, but the largest DEI occurred in 1975, followed by 1984, 1913, and 2010. The most extreme drought year was 1975, followed by 1984, 2010, and 1913 (Table S2). For autumn, the most extreme drought year was 1909, with both the highest drought intensity and largest drought extent. This year was followed by 2005, 1915, and 1910 (Table S2).

Figure S2 shows the spatial pattern of the mean DIIs of the ten extreme drought years for each season, as listed in Table S2. We found that the hotspots of extreme droughts varied with season. For winter, the most severe droughts occurred from approximately the central to southern part of the study area, with SPIs of −1.5 to −2. This area includes southeastern Kazakhstan, eastern Uzbekistan, and southwestern Kazakhstan to the west of Uzbekistan. In

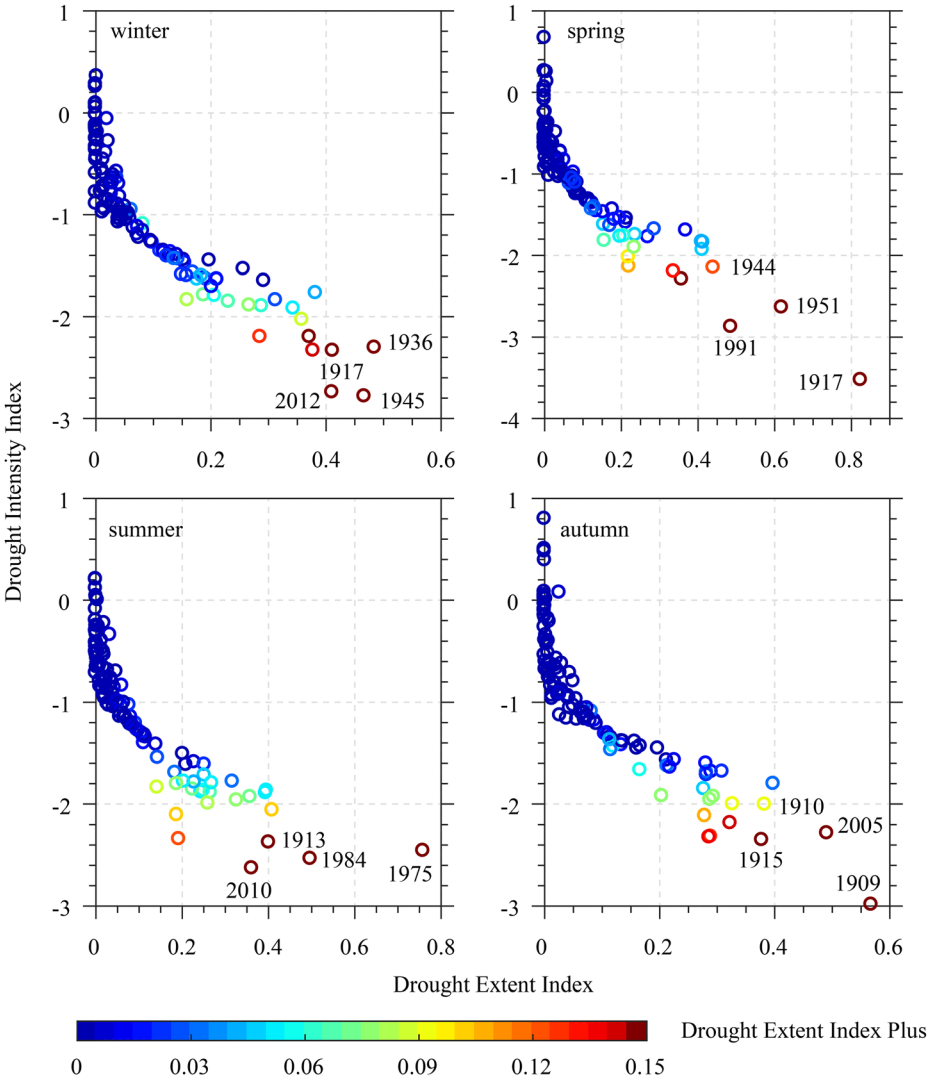

Fig. 2 Joint distribution of regional drought extent and drought intensity for each season

the northern and southern parts of the study area, the drought intensity was weak, with SPIs less than −0.5 for most areas. For spring and summer, severe droughts were spread extensively over the study area and had much larger extents than in winter. In spring, the most severe droughts occurred in the middle of the study area. In summer, the most severe droughts occurred over two areas. One center was located in the central-northern part of the study area, and the other center was located in the middle of the study area. For autumn, the drought intensity was weaker than that in the other three seasons, and the mean severe drought extent was also smaller than that in the other three seasons. Moreover, there was no clear drought center in autumn, although the drought intensity exhibited spatial variability. There were higher mean DIIs in the northwest corner and in some areas of the central-south part of the study area than in other regions.

3.3 Correlations between drought intensity/extent and large-scale climate anomalies

Table 1 shows that the variations in DII and DEI were correlated with anomalies in large-scale atmospheric circulation and the tropical Pacific SST; however, the strengths of these correlations varied with seasons and climate patterns. For winter, both the DII and DEI were significantly correlated with AO, EA, EAWR, Niño 4 and Niño 3.4 SST. Intensified drought and extensive drought mostly occurred in the negative phase of the AO, EA, and EAWR patterns as well as in the cold phase of the tropical central-eastern Pacific. Among these items, the strongest correlations occurred with the EA and EAWR patterns, one of which may explain approximately 16% of the variance in the DII and 12–13% of the variance in the DEI. Figure 3 confirms the strong links to large-scale atmospheric circulation anomalies. It shows that extensive and intensified drought occurred in the atmospheric wave train over the mid- to high-latitudes of the Atlantic–Eurasian region, which has high resemblance to the negative phase of the EAWR pattern, as well as in the atmospheric dipole pattern over the East Atlantic of the Northern Hemisphere, which has high resemblance to the negative phase of the EA pattern (Lim 2015; Gao et al. 2017).

Secondary strong correlations occurred with the Niño 4 and Niño 3.4 SST, which may explain approximately 8–10% of the variance in the DII. The correlation with the Niño 4 SST was stronger than that with the Niño 3.4 SST. The DII may be more closely linked to the tropical central Pacific than to the tropical eastern Pacific. This feature is confirmed by Fig. 4, which shows both DII and DEI were significantly correlated with tropical Pacific SST. Additionally, Fig. 4 shows that drought intensity and extent were also closely linked to the tropical Indian Ocean and subtropical Atlantic SST.

For spring, both the DII and DEI were significantly correlated with the EA, EAWR, Niño 4 and Niño 3.4 SST. These correlations also suggest that intensified and extensive drought mostly occurred in the negative phase of the EA and EAWR patterns as well as in the cold phase of the tropical Pacific. It is consistent with the above-mentioned results for winter. Additionally, for the DEI, there were significant correlations with the NAO pattern as well as the PDO pattern. Among these items, the strongest correlations occurred with the EAWR and Niño 4 SST, one of which may explain 16–17% of the variance in the DII and 10–12% of the variance in the DEI. The secondary correlations occurred with the EA pattern and Niño 3.4 SST.

Table 1 Correlation coefficients of the drought intensity index (DII) and drought extent index (DEI) against large-scale atmospheric circulation patterns and SST anomalies

Season	Winter		Spring		Summer		Autumn	
Index	DII	DEI	DII	DEI	DII	DEI	DII	DEI
AMO	−0.09	0.03	0.18	−0.11	0.12	−0.12	0.04	−0.08
AO	**0.25****	**−0.23***	0.08	−0.12	−0.14	0.1	**0.2***	**−0.2***
EA	**0.4****	**−0.34****	**0.25***	**−0.25***	0.14	**−0.28***	**0.36****	**−0.23***
EAWR	**0.41****	**−0.37****	**0.42****	**−0.32****	0.01	0.07	0.09	−0.17
NAO	0.11	−0.11	0.18	**−0.21***	−0.02	0.03	0.13	−0.09
Niño 3.4 SST	**0.29****	**−0.21***	**0.31****	**−0.27****	0.08	−0.09	**0.31****	**−0.2***
Niño 4 SST	**0.32****	**−0.23***	**0.4****	**−0.34****	**0.21***	**−0.22***	**0.36****	**−0.27****
PDO	0.11	−0.1	0.15	**−0.19***	0.1	−0.05	0.07	−0.06
POEA	−0.06	0.09	−0.07	0.08	−0.2	0.16	−0.08	0.04
SCAND	−0.04	0.04	0.2	−0.19	**−0.26***	0.23	0.17	−0.05

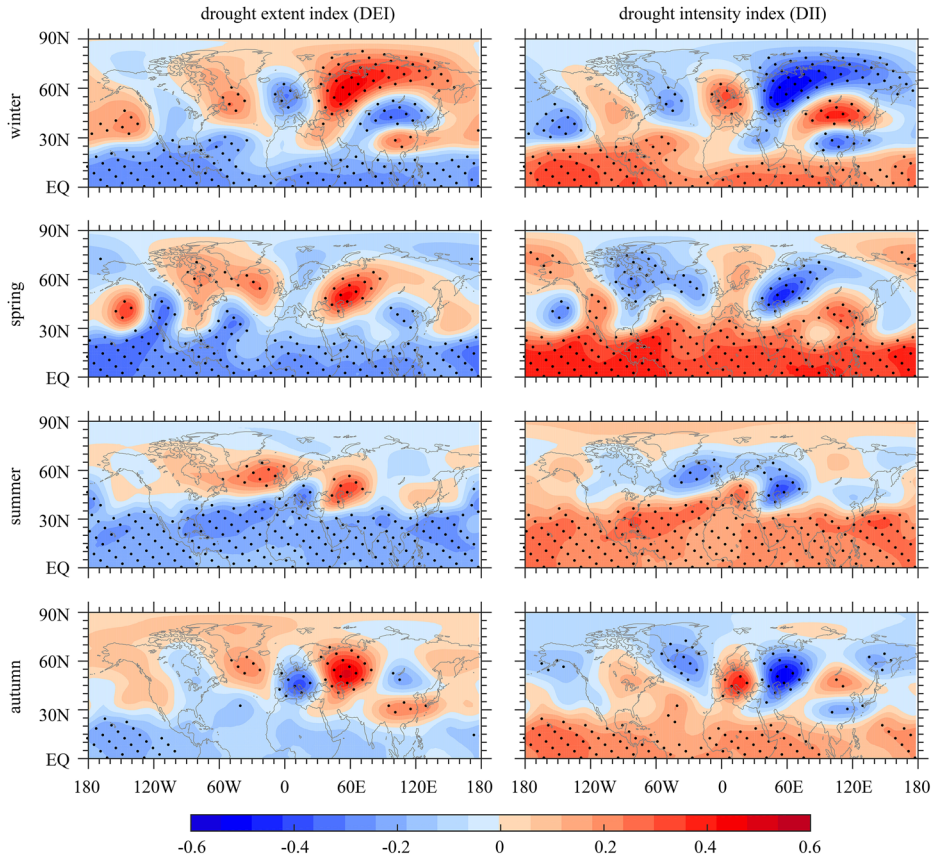

Fig. 3 Correlations between geopotential heights at a pressure level of 200 hPa and the drought extent index (DEI) and drought intensity index (DII) of Central Asia from 1902 to 2015 for each season (black dots denote significance at a level of 0.05)

Consistent with winter, the drought intensity and extent were more closely linked to the tropical central Pacific SST than the tropical eastern Pacific SST. Figure 4 also confirms that extensive drought was linked to cooling tropical oceans, including the central Pacific and Indian Ocean, as well as cooling of the subtropical Atlantic Ocean. In contrast to winter, drought intensity and extent were more closely linked to the EAWR than the EA pattern. Figure 3 also shows that extensive and intensified drought may have occurred with the wave train pattern over the mid- to high latitudes of the Atlantic Ocean to Eurasian land areas, closely matching the negative phase of the EAWR pattern (Lim 2015; Gao et al. 2017). The dipole pattern over the East Atlantic Ocean of the Northern Hemisphere closely matches the negative phase of the EA pattern that remained but with a weak signal, which was mainly derived from non-significant correlations at its east center (Fig. 3).

For summer, both the DII and DEI were simultaneously correlated with only the Niño 4 SST. The intense and extensive drought mostly occurred in the cold phase of the tropical central Pacific. Figure 4 also confirms that there was a significant correlation in only the tropical central Pacific SST. For the large-scale atmospheric circulation patterns, there were weak correlations for the EA pattern with only the DEI and SCAND patterns with only the

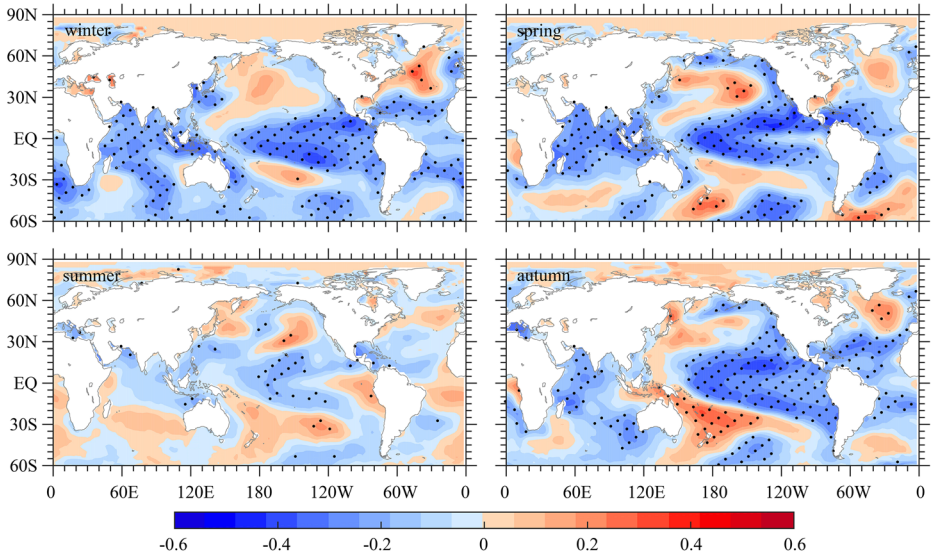

Fig. 4 Correlations between SST and the DEI of Central Asia from 1902 to 2015 for each season (black dots denote significance at a level of 0.05)

DII. Figure 3 shows that the wave train structure and dipole structure in winter and spring did not occur in summer. The summer regional drought may be weakly linked to large-scale atmospheric circulation anomalies over mid- to high latitudes.

For autumn, both the DII and DEI were significantly correlated with EA, AO, Niño 4 and Niño 3.4 SST. Intense and extensive drought mostly occurred in the negative phase of the EA and AO patterns as well as in the cold phase of the tropical central-eastern Pacific. Among these items, the strongest correlations occurred with the EA and Niño 4 SST, one of which may explain 13% of the variance in the DII and 5–7% of the variance in the DEI. The secondary correlations occurred with the AO and Niño 3.4 SST. It is consistent with the above three seasons that drought is more closely linked to the tropical central Pacific SST than to the tropical eastern Pacific. Figure 4 confirms the close link to the tropical central Pacific; however, the strength of the link to the Indian Ocean in autumn is much lower than that in winter and spring.

The close link to the EA pattern is also confirmed by Fig. 3. There is an approximately meridional dipole structure over the Eastern Atlantic Ocean that matches the EA pattern (Lim 2015; Gao et al. 2017). Figure 3 also explains why there was no significant correlation with the EAWR pattern. There is a wave chain structure over the mid- to high latitudes. However, in comparison to that in winter, the correlations were nonsignificant over East Asia and North America, and the center over Central Asia, i.e., approximately 60°E, was much smaller than that in winter, and the center over Europe moved southeastward to southern Europe. These differences lead to this wave chain-like structure mismatching with the EAWR pattern. Hence, the nonsignificant correlations with the EAWR pattern could be explained.

The above findings indicate that winter drought was strongly linked to both the negative EA and EAWR patterns, while spring and autumn droughts were strongly linked to the negative EAWR and EA patterns, respectively. In fact, the hotspots where the SPI was correlated with the EA and EAWR varied with season. Figure S3 shows that in winter, the significant correlations between SPI and EA index mainly exist in the northeastern sector,

while in autumn, they extend beyond the northeastern sector to the southwestern sector. In winter, the significant correlations between SPI and the EAWR index exist over most of the study area except for the eastern margin sector and high correlation centers exist in the western and central sectors, while in spring, they mainly exist over the central-eastern sector. Compared to the EA pattern and EAWR pattern, the area where the SPI is highly sensitive to Niño 4 SST mainly exists in the southern sector, through three seasons: winter, spring, and autumn (Fig. S3). As an exception, in summer, the high correlation areas exist in only the limited southeast sector and northeast sector. These findings suggest that response sensitivities of precipitation to the EA, EAWR, and Niño 4 SST vary with subregions; high correlations between DII and DEI and EA, EAWR and Niño 4 SST are actually realized in different ways.

3.4 Large-scale atmospheric circulation anomalies for extreme drought years

Figure 5 shows the composite mean large-scale geopotential height anomalies for the ten extreme drought years shown in Table S2. There were large differences among the seasons. In winter, the extreme droughts were accompanied by a dipole pattern anomaly over the Atlantic Ocean with a positive center over southern Greenland and a negative center around the Azores Islands. A north-by-west to south-by-east pressure gradient exists over the Atlantic Ocean, which is highly consistent with the negative EA pattern and slightly similar to the negative NAO pattern. There were no wave chain structures of the EAWR pattern, which was significantly correlated with inter-annual variations in DEIs and DIIs. Hence, the EAWR index covaried with normal variations in the DII and DEI but not with their extremes, while the EA index covaried with both the normal variations and extremes of the DII and DEI. The negative EA pattern may play a crucial role in extreme drought.

In spring, the geopotential height anomalies are dominantly characterized by wave trains across the mid- to high-latitudes of the Northern Hemisphere. In particular, over the Atlantic Ocean and Eurasia, there are two low anomaly centers and two high anomaly centers. Low

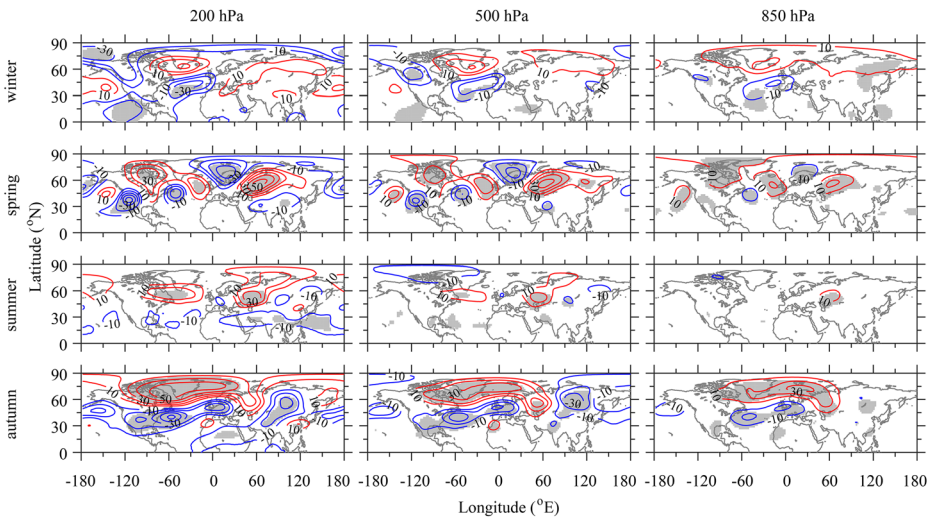

Fig. 5 Geopotential height anomalies (units: gpm) for the ten extreme drought years in Central Asia for each season, referring to the climatological means of the other years from 1902 to 2015 (shading denotes significance at a level of 0.05)

anomaly centers exist over the midlatitude western Atlantic Ocean and Northwest Europe, while high anomaly centers exist over the eastern Atlantic Ocean and at the junction of Europe–Asia. Such a pattern has high resemblance to the negative EAWR pattern. Hence, the EAWR pattern covaried with not only the normal variations in the DIIs and DEIs but also their extremes. Both normal drought and extreme drought may be linked to the negative EAWR pattern.

In summer, the geopotential height anomalies are mainly characterized by anomalies over the subtropical region, with a significant low anomaly over the southern portion of Eurasian land and a significant high anomaly over Central Asia and the Northwest Atlantic Ocean at the pressure level of 200 hPa. Down to pressure levels of 500 hPa and 850 hPa, there are locally high anomalies over Central Asia with no other anomaly. These findings suggest that extreme drought in summer may be very weakly linked to large-scale atmospheric oscillations.

In autumn, there is a high anomaly over high latitudes of the Arctic Polar area, with a center over the North Atlantic Ocean, and a low anomaly over the subtropical Atlantic Ocean at a pressure level of 200 hPa. This pattern looks similar to the negative AO pattern. Down to 500 hPa and 800 hPa, there is a dipole structure over the Atlantic Ocean, with a positive center in the north and a negative center in the south. In particular, the north center spreads across the entire high-latitude North Atlantic Ocean to North Europe, while the south center occupies a smaller extent than the north center and exhibits two sub-centers in the subtropic western Atlantic Ocean and western Europe. Such a spatial pattern matches the negative AO pattern well. Hence, the extreme drought in autumn may be closely linked to the negative AO pattern. However, the EA pattern is not shown clearly. The EA pattern may covary with the normal variations in the DEI and DII but not with their extremes.

4 Discussion

This study focused on the regional drought for each season and the entirety of Central Asia, including five states of the former Soviet Union, rather than only some parts of Central Asia. More importantly, the yearly variations in the regional drought intensity and extent are depicted, and the large-scale climate patterns linked with drought are highlighted for each season. The results show that the variations in the DEI and DII from 1902 to 2015 differed among the seasons. On the one hand, the decadal to multidecadal variations are different among the seasons; on the other hand, the extreme drought years are also different among the seasons. There were some distinguished extreme droughts, such as in 1917 and 1945 (Zhang et al. 2017; Chen and Huang 2017), between 1975 and 1977 (Sheffield and Wood 2011; Guo et al. 2018b), and in 2006, 2008, and 2010 (Xu et al. 2016). This study does not only detect these droughts but also, more importantly, clarifies their seasonality. The droughts in 1917 and 1945 mainly occurred in winter and spring, the drought in 1975–1977 mainly occurred in summer, and droughts in 2006 and 2008 mainly occurred in summer and autumn.

The results also show that the dominant large-scale climate patterns linked with drought were not exactly the same among the seasons. Such discrepancies may be essentially derived from changes in atmospheric circulation along with the annual cycle of insolation and heating on Earth (Schiemann et al. 2008). Bothe et al. (2012) reported that climatological atmospheric circulation patterns over the Northern Hemisphere change with seasons, and as a consequence, the water vapor flux paths to Eurasian land also vary with seasons.

The drought in each season was closely linked to the cooling tropical central-eastern Pacific, i.e., the anomalously low Niño 3.4 SST, and was also closely linked to both negative EAWR and EA patterns but with seasonal differences. In spring and winter, drought was linked to the negative EAWR pattern, while in winter and autumn, it was linked to the negative EA pattern. The close link to cooling tropical central-eastern Pacific could be explained by the idea that La Niña may be unfavorable for Central Asia precipitation due to the enhancement of tropical Indo-West Pacific Ocean convection, resulting in increases in diabatic heating, which excite baroclinic and barotropic stationary Rossby waves over central-southwest Asia and the Middle East (e.g., Barlow et al. 2002, 2016; Hoell et al. 2012; Hoell and Funk 2013; Rana et al. 2019). In particular, our result is also consistent with Schubert et al. (2016), who reported that the closest link to the cooling tropical central-eastern Pacific occurs in spring (March to May).

The importance of EAWR pattern on Central Asia drought, in particular, in winter and spring could also be supported by the previous finding that less precipitation would exist in the negative EAWR pattern in the boreal winter half-year (Rana et al. 2019). The negative EAWR pattern favors weather types associated with a Rossby ridge over Central Asia, which implies a northward shift of westerly moisture fluxes and is favorable for surface anticyclonic activities reducing moisture transport from the Arabian Sea and Persian Gulf and, ultimately, suppressing precipitation (Barlow et al. 2016; Gerlitz et al. 2018; Rana et al. 2019). The effects of EAWR may be partly contributed by the effects of ENSO, since it may modulate extratropical atmosphere teleconnections (Hurrell 1996). This issue has been addressed by Yin et al. (2014), who reported that significant correlations existed between the EAWR index and Niño 3.4 index ($r = 0.40$, $p < 0.05$). Moreover, partial correlations still existed between the EAWR and westerly index (WI) with the concurrent Niño 3.4 index as the control variable, reaching as high as $r = 0.52$ ($p < 0.01$), which is comparable to the normal correlation ($r = 0.58$, $p < 0.01$). Therefore, the effects of the EAWR pattern on the westerly jet stream should be considered independently from those of ENSO. Because the westerly jet stream plays a crucial role in Central Asia precipitation, the effects of EAWR on Central Asia precipitation may also be independent of those of ENSO.

In addition to the EAWR pattern, Central Asia precipitation is also significantly correlated with other atmospheric teleconnections, such as the POEA pattern (Yin et al. 2014), NAO pattern (Syed et al. 2010), AO pattern (Gerlitz et al. 2018), SCAND pattern (de Beurs et al. 2018), and EA pattern (Bothe et al. 2012; Bastos et al. 2016). These patterns are extratropical teleconnections, and their effects on Central Asia precipitation are mostly realized by regulating the locations of westerly jet streams, which may alter the water vapor supply pathway to inland Eurasia and hence the water vapor amount transported to Central Asia (see review by Gerlitz et al. 2018). The results from this study confirm that drought was linked to a negative EA pattern and AO pattern. Furthermore, in spring the links to the EA and EAWR patterns were comparable in strength with each other, and in autumn, the link to the EA pattern was closer than that to the EAWR pattern. However, links to the POEA, NAO, and SCAND patterns were not detected in this study, which may be explained partly by the fact that the effects of these teleconnection models on Central Asia precipitation are asymmetric (Bother 2012). For instance, a positive NAO pattern is favorable for increased precipitation, while no significant relationship between the negative NAO pattern and less precipitation was detected (Gerlitz et al. 2018).

The existing studies mostly paid attention to the boreal winter half-year and not to summer because summer is a less rainy season in Central Asia. Herein, we found that the extent and

intensity of summer drought also exhibited large interannual and decadal variations; however, summer drought was only slightly linked to extratropical atmospheric teleconnection. It is prominent that extensive and intense drought mostly occurred under only local anomalous high-pressure conditions over the study area, which is consistent with the localized anticyclonic anomaly between the Aral Sea and Lake Balkash (Bothe et al. 2012). On the long-term trend since the 1970s, the declining trend of drought intensity and drought extent may also be linked to anthropogenic forcing (Peng et al. 2018). Many more studies are needed to clarify the potential climate dynamics modulating summer drought intensity and extent.

Notably, we considered only the seasonal scale (i.e., three continuous months) SPI when analyzing drought variations. It might be worthwhile to research different timescales of the SPI to reveal the drought variations across multiple timescales. Additionally, the drought represented by low SPI values was mostly caused by precipitation deficiencies. However, in arid and semiarid regions, both precipitation and other factors, such as evapotranspiration, wind, and solar radiation, may play important roles on drought (Dai 2011). As such, it is also worthy to use drought indices (SPEI, PDSI, scPDSI, etc.) that are determined by both precipitation and evapotranspiration to reveal the characteristics of severe drought events in Central Asia.

5 Summary

The above results show that the regional drought intensity and extent exhibited large interannual and interdecadal variability from 1902 to 2015 but with large discrepancies among the seasons. The variations in the DIIs and DEIs were significantly correlated with the tropical central-eastern Pacific Ocean SST for each season and extratropical atmospheric teleconnections, including the EAWR, EA, and AO patterns, but with discrepancies among the seasons. In winter, both negative EA and EAWR patterns played comparably important roles; in spring, the influence of a negative EAWR pattern was the most prominent, while in autumn, it was a negative EA pattern. The cooling tropical central-eastern Pacific and these extratropical atmospheric teleconnections modify atmospheric circulations in different ways, but there is a common result that the water vapor supply to Central Asia is reduced.

These results confirm and improve upon previous results, as the discrepancies among the seasons were highlighted. The discrepancies are observed in the divergent temporal variations in drought extent and drought index as well as in divergent large-scale climate patterns potentially leading to drought. These results also suggest that the large-scale climate patterns potentially responsible for normal drought and for extreme drought are different in winter and autumn. The results may be valuable for drought attributions and drought projections at seasonal scale. More studies are also needed to improve our understanding of drought patterns. For instance, it would be valuable to enhance the study of summer drought and quantify drought using other drought indices, such as the PDSI and SPEI.

Supplementary Information The online version contains supplementary material available at https://doi.org/10.1007/s10584-021-03131-y.

Acknowledgments This research was supported by the Strategic Priority Research Program of the Chinese Academy of Sciences (XDA20020202), the National Natural Science Foundation of China (41790424), the Key Program from CAS (ZDRW-ZS-2017-4), and the Key Program from CAS (QYZDBSSW-DQC005). The gridded precipitation dataset was available through the Climatic Research Unit, University of East Anglia (CRU), and the atmospheric circulation datasets, including geopotential height, meridional, and zonal wind,

were available through the NOAA-CIRES twentieth Century Reanalysis dataset (https://psl.noaa.gov/data/20thC_Rean/). The atmospheric circulation indices and SST indices were acquired from the website at https://www.esrl.noaa.gov/psd/data/climateindices/list/.

Author's contributions XZ and QG designed the research; MH and MB analyzed the data and illustrated the plots; XZ wrote the paper. QG revised the original paper.

Funding Strategic Priority Research Program of the Chinese Academy of Sciences (XDA20020202);
National Natural Science Foundation of China (41790424);
Key Program from CAS (ZDRW-ZS-2017-4; QYZDBSSW-DQC005);

Availability of data and materials All used data and materials have been described in detail in the manuscript.

Declarations

Competing interests The authors declare that they have no conflicts of interest.

Code availability Not applicable.

Ethical approval Not applicable.

Consent to participate Not applicable.

Consent to publish Yes

References

Andreadis KM, Clark EA, Wood AW et al (2005) Twentieth-century drought in the conterminous United States. J Hydrometeorol 6(6):985–1001. https://doi.org/10.1175/JHM450.1

Ashraf M, Routray JK (2015) Spatio-temporal characteristics of precipitation and drought in Balochistan Province, Pakistan. Nat Hazards 77(1):229–254. https://doi.org/10.1007/s11069-015-1593-1

Barlow M, Cullen H, Lyon B (2002) Drought in central and Southwest Asia: La Niña, the warm pool, and Indian Ocean precipitation. J Clim 15:697–700

Barlow M, Zaitchik B, Paz S et al (2016) A review of drought in the Middle East and Southwest Asia. J Clim 29(23):8547–8574. https://doi.org/10.1175/JCLI-D-13-00692.1

Bastos A, Coauthors (2016) European land CO_2 sink influenced by NAO and East-Atlantic pattern coupling. Nat Commun 7:10315. https://doi.org/10.1038/ncomms10315

Bothe O, Fraedrich K, Zhu XH (2012) Precipitation climate of Central Asia and the large-scale atmospheric circulation. Theor Appl Climatol 108(3-4):345–354. https://doi.org/10.1007/s00704-011-0537-2

Chen FH, Huang W (2017) Multi-scale climate variations in the arid Central Asia. Adv Clim Chang Res 8(1):1–2. https://doi.org/10.1016/j.accre.2017.02.002

Dai AG (2011) Characteristics and trends in various forms of the palmer drought severity index during 1900-2008. J Geophys Res Atmos 116:D12115. https://doi.org/10.1029/2010JD015541

Damberg L, AghaKouchak A (2014) Global trends and patterns of droughts from space. Theor Appl Climatol 117(3):441–448. https://doi.org/10.1007/s00704-013-1019-5

de Beurs KM, Henebry GM, Owsley BC et al (2018) Large scale climate oscillation impacts on temperature, precipitation and land surface phenology in Central Asia. Environ Res Lett 13(6):065018. https://doi.org/10.1088/1748-9326/aac4d0

Deng HJ, Chen YN (2017) Influences of recent climate change and human activities on water storage variations in Central Asia. J Hydrol 544:46–57. https://doi.org/10.1016/j.jhydrol.2016.11.006

Farah P (2015) Energy security, water resources, environmental concerns and economic development in Central Asia. World Scientific, London

Ganguli P, Ganguly AR (2016) Robustness of meteorological droughts in dynamically downscaled climate simulations. J Am Water Resour Assoc 52(1):138–167. https://doi.org/10.1111/1752-1688.12374
Gao T, Yu J, Paek H (2017) Impacts of four northern-hemisphere teleconnection patterns on atmospheric circulations over Eurasia and the Pacific. Theor Appl Climatol 129:815–831. https://doi.org/10.1007/s00704-016-1801-2
Gerlitz L, Steirou E, Schneider C et al (2018) Variability of the cold season climate in Central Asia. Part I: weather types and their tropical and extratropical drivers. J Clim 31(18):7185–7207. https://doi.org/10.1175/JCLI-D-17-0715.1
Guan XF, Yang LM, Zhang YX et al (2019) Spatial distribution, temporal variation, and transport characteristics of atmospheric water vapor over Central Asia and the arid region of China. Glob Planet Change 172:159–178. https://doi.org/10.1016/j.gloplacha.2018.06.007
Guo H, Bao AM, Liu T et al (2018a) Spatial and temporal characteristics of droughts in Central Asia during 1966–2015. Sci Total Environ 624:1523–1538. https://doi.org/10.1016/j.scitotenv.2017.12.120
Guo H, Bao AM, Ndayisaba F et al (2018b) Space-time characterization of drought events and their impacts on vegetation in Central Asia. J Hydrol 564:1165–1178. https://doi.org/10.1016/j.jhydrol.2018.07.081
Harris I, Jones PD, Osborn TJ et al (2014) Updated high-resolution grids of monthly climatic observations - the CRU TS3.10 dataset. Int J Climatol 34(3):623–642. https://doi.org/10.1002/joc.3711
Heim RR (2002) A review of twentieth-century drought indices used in the United States. Bull Am Meteorol Soc 83(8):1149–1165. https://doi.org/10.1175/1520-0477-83.8.1149
Hoell A, Funk C (2013) The ENSO-related West Pacific Sea surface temperature gradient. J Clim 26:9545–9562. https://doi.org/10.1175/JCLI-D-12-00344.1
Hoell A, Barlow M, Saini R (2012) The leading pattern of intraseasonal and interannual Indian Ocean precipitation variability and its relationship with Asian circulation during the boreal cold season. J Clim 25:7509–7526. https://doi.org/10.1175/JCLI-D-11-00572.1
Hu ZY, Zhou QM, Chen X et al (2017) Variations and changes of annual precipitation in Central Asia over the last century. Int J Climatol 37(S1):157–170. https://doi.org/10.1002/joc.4988
Hu ZY, Zhou QM, Chen X et al (2018) Evaluation of three global gridded precipitation data sets in Central Asia based on rain gauge observations. Int J Climatol 38(9):3475–3493. https://doi.org/10.1002/joc.5510
Hua LJ, Zhong LH, Ma ZG (2017) Decadal transition of moisture sources and transport in northwestern China during summer from 1982 to 2010. J Geophys Res Atmos 122(23):522–540. https://doi.org/10.1002/2017JD027728
Hurrell JW (1996) Influence of variations in extratropical wintertime teleconnections on northern hemisphere temperature. Geophys Res Lett 23:665–668
Li Z, Chen YN, Wang Y et al (2016) Dynamic changes in terrestrial net primary production and their effects on evapotranspiration. Hydrol Earth Syst Sci 20(6):2169–2178. https://doi.org/10.5194/hess-20-2169-2016
Lim Y-K (2015) The East Atlantic/West Russia (EA/WR) teleconnection in the North Atlantic: climate impact and relation to Rossby wave propagation. Clim Dyn 44(11-12):3211–3222. https://doi.org/10.1007/s00382-014-2381-4
Lioubimtseva E, Henebry GM (2009) Climate and environmental change in arid Central Asia: impacts, vulnerability, and adaptations. J Arid Environ 73(11):963–977. https://doi.org/10.1016/j.jaridenv.2009.04.022
Mitchell TD, Jones PD (2005) An improved method of constructing a database of monthly climate observations and associated high-resolution grids. Int J Climatol 25(6):693–712. https://doi.org/10.1002/joc.1181
Peng D, Zhou T, Zhang L, Wu B (2018) Human contribution to the increasing summer precipitation in Central Asia from 1961 to 2013. J Clim 31(19):8005–8021. https://doi.org/10.1175/JCLI-D-17-0843.1
Rana S, McGregor J, Renwick J (2019) Dominant modes of winter precipitation variability over central Southwest Asia and inter-decadal change in the ENSO teleconnection. Clim Dyn 53(9-10):5689–5707. https://doi.org/10.1007/s00382-019-04889-9
Schiemann R, Luthi D, Vidale PL et al (2008) The precipitation climate of Central Asia-intercomparison of observational and numerical data sources in a remote semiarid region. Int J Climatol 28(3):295–314. https://doi.org/10.1002/joc.1532
Schubert SD, Stewart RE, Wang H et al (2016) Global meteorological drought: a synthesis of current understanding with a focus on SST drivers of precipitation deficits. J Clim 29(11):3989–4019
Sheffield J, Wood EF (2011) Drought: past problems and future scenarios. Taylor and Francis, London, p 210
Sheffield J, Andreadis KM, Wood EF et al (2009) Global and continental drought in the second half of the twentieth century: severity-area-duration analysis and temporal variability of large-scale events. J Clim 22(8):1962–1981. https://doi.org/10.1175/2008JCLI2722.1
Slivinski LC, Compo GP, Whitaker JS et al (2019) Towards a more reliable historical reanalysis: improvements for version 3 of the twentieth century reanalysis system. Quart J Roy Meteor Soc 145(724):2876–2908. https://doi.org/10.1002/qj.3598

Sugg M, Runkle J, Leeper R et al (2020) A scoping review of drought impacts on health and society in North America. Clim Chang 162:1177–1195. https://doi.org/10.1007/s10584-020-02848-6

Syed FS, Giorgi F, Pal JS, Keay K (2010) Regional climate model simulation of winter climate over central–Southwest Asia, with emphasis on NAO and ENSO effects. Int J Climatol 30:220–235. https://doi.org/10.1002/joc.1887

Tao H, Borth H, Fraedrich K et al (2014) Drought and wetness variability in the Tarim River basin and connection to large-scale atmospheric circulation. Int J Climatol 34:2678–2684. https://doi.org/10.1002/joc.3867

Vicente-Serrano SM, Quiring SM, Pena-Gallardo M et al (2020) A review of environmental droughts: increased risk under global warming? Earth Sci Rev 201:102953. https://doi.org/10.1016/j.earscirev.2019.102953

Xu GB, Liu XH, Trouet V et al (2019) Regional drought shifts (1710–2010) in East Central Asia and linkages with atmospheric circulation recorded in tree-ring $\delta^{18}O$. Clim Dyn 52(1-2):713–727. https://doi.org/10.1007/s00382-018-4215-2

Xu HJ, Wang XP, Zhang XX (2016) Decreased vegetation growth in response to summer drought in Central Asia from 2000 to 2012. Int J Appl Earth Obs Geoinf 52:390–402. https://doi.org/10.1016/j.jag.2016.07.010

Yin ZY, Wang H, Liu X (2014) A comparative study on precipitation climatology and interannual variability in the lower midlatitude East Asia and Central Asia. J Clim 27:7830–7848. https://doi.org/10.1175/JCLI-D-14-00052.1

Zhai JQ, Huang JL, Su BD et al (2017) Intensity–area–duration analysis of droughts in China 1960–2013. Clim Dyn 48:151–168. https://doi.org/10.1007/s00382-016-3066-y

Zhang RB, Zhang TW, Kelgenbayev N et al (2017) A 189-year tree-ring record of drought for the Dzungarian Alatau, arid Central Asia. J Asian Earth Sci 148:305–314. https://doi.org/10.1016/j.jseaes.2017.05.003

Zhao Y, Huang AN, Zhou Y et al (2014) Impact of the middle and upper tropospheric cooling over Central Asia on the summer rainfall in the Tarim Basin, China. J Clim 27(12):4721–4732. https://doi.org/10.1175/JCLI-D-13-00456.1

Zhao Y, Zhang HQ (2016) Impacts of SST warming in tropical Indian Ocean on CMIP5 model-projected summer rainfall changes over Central Asia. Clim Dyn 46(9-10):3223–3238. https://doi.org/10.1007/s00382-015-2765-0

Zhou Y, Huang AN, Zhao Y et al (2015) Influence of the sea surface temperature anomaly over the Indian Ocean in march on the summer rainfall in Xinjiang. Theor Appl Climatol 119(3-4):781–789. https://doi.org/10.1007/s00704-014-1149-4

Affiliations

Xuezhen Zhang [1,2] · Miao He [1,2] · Mengxin Bai [1,2] · Quansheng Ge [1]

[1] Key Laboratory of Land Surface Pattern and Simulation, Institute of Geographic Sciences and Natural Resources Research, Chinese Academy of Sciences, Beijing 100101, China

[2] University of Chinese Academy of Sciences, Beijing 100049, China